

High redshift evolution of optically and IR-selected galaxies: a comparison with CDM scenarios

Adriano Fontana¹, Nicola Menci¹, Sandro D’Odorico², Emanuele Giallongo¹, Francesco Poli¹, Stefano Cristiani^{3,4}, Alan Moorwood², Paolo Saracco⁵

¹ Osservatorio Astronomico di Roma, 00040 Monte Porzio, Italy

² European Southern Observatory, 85748 Garching bei München, Germany

³ Dipartimento di Astronomia dell’ Università, 35122 Padova, Italy

⁴ Space Telescope European Coordinating Facility, European Southern Observatory, 85748 Garching bei München, Germany

⁵ Osservatorio Astronomico di Brera, 22055 Merate (LC) Italy

24 March 2018

ABSTRACT

A combination of ground-based (NTT and VLT) and HST (HDF-N and HDF-S) public imaging surveys have been used to collect a sample of 1712 I-selected and 319 $K \leq 21$ galaxies observed with an extended spectral coverage from the U to the K band. Photometric redshifts have been obtained for all these galaxies, using a spectral library computed from Bruzual and Charlot models. The results have been compared with the prediction of an analytic rendition of the current CDM hierarchical models for galaxy formation that explicitly accounts for magnitude limits and dust extinction. We focus in particular on two observed quantities: the galaxy redshift distribution at $K \leq 21$ and the evolution of the UV luminosity density. The former has been proposed by Kauffmann and Charlot (1998) as a very robust prediction of any CDM hierarchical model, and we show that it is remarkably constant among different cosmological models. The derived photometric redshift distribution is in agreement with the hierarchical CDM prediction, with a fraction of only 5% of galaxies detected at $z \geq 2$. This result strongly supports hierarchical scenarios where present-day massive galaxies are the result of merging processes. The observed UV luminosity density in our I-selected sample is confined within a factor of 4 over the whole range $0 < z < 4.5$, in agreement with previous spectroscopic and photometric surveys. CDM models in a critical ($\Omega = 1, \Lambda = 0$) Universe are not able to produce the density of UV photons that is observed at $z \geq 3$. CDM models in Λ -dominated universe are in better agreement at $3 \leq z \leq 4.5$, but predict a pronounced peak at $z \simeq 1.5$ and a drop by a factor of 8 from $z = 1.5$ to $z = 4$ that is not observed in the data. We conclude that improvements are required in the treatment of the physical processes directly related to the SFR, e.g. the starburst activity in merger processes and/or different recipes for linking the supernovae feedback to the star formation activity.

1 INTRODUCTION

Understanding how massive galaxies formed and evolved is one of the major goals of present-day cosmology. Currently favoured theoretical scenarios attempt to describe “*ab initio*” the global formation and evolution of galaxies from primordial fluctuations including the main physical processes involved (e.g. Kauffmann, White & Guiderdoni 1993, Cole et al 1994, Baugh et al 1998). These “hierarchical” models naturally predict galaxies to form from smaller units that accrete gas and merge to build up present-day massive objects. These models are challenged by several observations suggesting that bulges and ellipticals were formed at a very early

stage of the Universe and slowly evolved thereafter (Bernardi et al 1999, Schade et al 1999 and references therein).

Kauffmann and Charlot (1998; KC98 hereafter) proposed the use of the redshift distribution of K-band limited samples to address this issue. The main advantage here is that the K band traces the IR radiation produced by ordinary stars at any $z \leq 4$ (see Fig. 1 of KC98) and is little affected by dust extinction, and it is therefore a reliable tracer of the mass in stars already assembled in galaxies at any redshift. As shown by KC98, hierarchical models prevent massive galaxies to be already assembled at $z \geq 1$, and the expected number of galaxies at $z \geq 1.5$ is about 4 times lower than the predictions of Pure Luminosity Evolution-

ary (PLE) models. Unfortunately, the existing spectroscopic surveys (Cowie et al. 1996, Cohen et al. 1999) still lack the required completeness at faint IR magnitudes in this critical redshift regime.

The evolution of the global star-formation rate as a function of z has long been recognized as a powerful tool to trace galaxy evolution. First results from spectroscopic (Lilly et al. 1995) and color-estimated (Madau et al 1996, 1998, Connolly et al 1997) redshift surveys suggested a steep rise and fall of the SFR with a main peak at $z \simeq 2$. Photometric redshift analysis (Giallongo et al 1998, G98 hereafter, Pascale et al 1999) and spectroscopic surveys at low and high z (Treyer et al. 1998, Cowie et al. 1999, Steidel et al. 1999), inclusion of dust corrections and far-IR detections (Hughes et al 1998) are now modifying this picture.

In this work we have used deep ground-based and HST multi-band observations from UV to IR to obtain photometric redshifts for galaxies in an optical ($I < 27.5$) and IR ($K < 21$) sample. The redshift distributions of the K-band limited sample and of the UV luminosity density have been compared with the results of the CDM models to test their fundamental properties.

2 THE BASIC INGREDIENTS: DATA AND MODELS

2.1 Multicolor catalogs

The observations used in this paper cover the full wavelength range from the UV to the K band and have sub-arcsec image quality. Two of the fields were observed with the ESO 3.5 NTT SUSI imager: the first (hereafter BR1202) is centered on the $z=4.7$ QSO BR1202-07, the second is a neighbouring field (NTT Deep Field, NTTDF hereafter). The BVRI images and catalogs of these fields are described in G98 and Arnouts et al (1999a) respectively, complemented by NTT observations in J and K (Saracco et al. 1999) and in the U band. The latter observations and the procedures to obtain the final UBVRJK catalogs are fully described in Fontana et al. (in preparation).

The third dataset results from the VLT-NICMOS observations of the HDF-S (Fontana et al 1999).

Finally, we have used the HDF-N and HDF-S with the IR observations obtained at Kitt Peak and at NTT-SOFI (Da Costa et al, 1998), respectively. For the HDF-N we have used the multicolor catalog published by Fernandez-Soto et al (1999), which uses an optimal technique to match the optical and IR images that have a quite different seeing. A similar catalog for the HDF-S has been provided by the same authors and is available at the WEB address <http://www.ess.sunysb.edu/astro/hfds/home.html>. Only WFPC bands have been used in the optical, for consistency with the HDF-N. In both cases we have clipped the outer regions of the frame with lower S/N.

Despite different origins, these data are sufficiently homogeneous for the purpose of the paper. Indeed, all catalogs have been obtained with similar procedures and software, and we have obtained photometric redshifts only for objects that are significantly above the detection threshold, so that small differences in the detection procedures are not expected to be important. All the multicolor catalogs use

the optical images as detection frame, as is appropriate for the estimate of the UV luminosity density at high redshift. We have also performed an independent object detection on the K images alone to ensure that all the galaxy at $K < 21$ were included in our optically-selected catalogs.

2.2 Photometric redshifts

The multicolor catalogs have been used to derive photometric redshifts for all the galaxies in the sample, using a code already described elsewhere (G98, Fontana et al in preparation). The code is based on the synthetic models of the Bruzual and Charlot GISSEL library, with the addition of intergalactic absorption (Madau et al 1996) and dust reddening (SMC-like Pei 1992). The accuracy on the HDF-N spectroscopic sample is $\sigma_z \sim 0.06(0.3)$ in the redshift interval $z = 0 - 1.5(1.5 - 3.5)$.

At fainter flux levels the reliability of photometric redshifts has been estimated with Monte Carlo simulations (Arnouts et al 1999b). We have defined a bright sample at $I_{AB} \leq 26$ that includes a subsample of the two HDFs and the NTTDF, and a fainter HDF(N+S) sample to $I_{AB} \leq 27.5$.

It is known that Galactic stars are significant sources of false high redshift candidates, especially in the brightest samples (Steidel et al 1999). Obvious stars have been excluded at $I_{AB} \leq 25.5$ in the HDF-S on the basis of the SExtractor morphological classification (Arnouts et al 1999a). The morphological selection removes all the $z \geq 5$ candidates in the HDF-S. These objects are typically bright ($I = 20 - 24$) and are always detected in the JHK bands. They would be formally assigned to $z \geq 5$ since they are nearly undetected in V and have a negative $J - K$, typical of M star spectra. Analogously, we have used the detailed morphological classification developed in Poli et al (1999) to identify stars down to $I_{AB} \simeq 25.3$ in the NTTDF sample.

2.3 An analytical rendition of hierarchical models

To compare these results with the present understanding of galaxy formation and evolution we have developed an analytical rendition of the hierarchical models (e.g. Cole et al. 1994). The prescription used to treat all the physical processes involved are identical to the "Durham" rendition, and we refer the reader to their list of papers for the details, while the complete formulations of our analytical rendition are given in Poli et al 1999 (see also Menci and Cavaliere 1999). Rather than following the history of each halo within a Monte Carlo scheme, we produce the statistical distributions of the main physical properties of galaxies in the DM halos. Our treatment extends the White and Frenk 1991 approach explicitly including the merging of galaxies in common halos through dynamical friction. This is accomplished by computing for all galaxies in DM halos the probability that the dynamical friction time is smaller than the halo survival time (as given by Lacey and Cole 1993). For the average quantities of interest here, this approach produces the same outputs as the "Durham" approach. We emphasize that we have not attempted to modify or improve the current models, that have several free parameters tuned to match the local properties of galaxies (counts, the I-band Tully-Fisher relation and the B-band luminosity function),

since our aim is simply to compare their prediction with the picture emerging from our data.

The only improvement introduced is a self-consistent treatment of the dust absorption, by defining an effective optical depth τ_λ (Guiderdoni & Rocca-Volmerange 1987) that is used to suppress the expected luminosity:

$$\tau_\lambda = \tau_{dust}^0 (1 - \omega)^{1/2} (A_\lambda/A_V) (Z_g/Z_\odot)^s f_g \quad (1)$$

where $(1 - \omega)^{1/2} (A_\lambda/A_V) (Z_g/Z_\odot)^s$ is a metal-dependent extinction law, f_g is the gas fraction $f_g = m_g/(m_g + m_*)$ (computed by the code) and τ_{dust}^0 is a gas-to-dust ratio chosen to match the observed B luminosity function at low redshift (Somerville and Primack 1998).

We adopt in this paper four different models, a Standard CDM (SCDM, $\Omega = 1, \Lambda = 0, h = 0.5$), an Open CDM ($\Omega = 0.5, \Lambda = 0, h = 0.7$), a low-density flat model (ΛCDM , $\Omega = 0.3, \Lambda = 0.7, h = 0.6$) and a tilted model, ($\Omega = 1, \Lambda = 0, h = 0.5$). The power spectrum normalization and the parameters that describe the IMF, the star formation process and the galaxy merging are taken from Heyl et al. (1995) for SCDM, Open and ΛCDM models, and from Poli et al (1999) for the tilted model.

3 THE $K \leq 21$ SAMPLES

The normalized cumulative redshift distributions of the 319 objects in the K -limited sample is shown in Fig.1. The upper panel shows the different distributions in the five fields considered here as well as the total distribution. The results from the five fields are clearly consistent, within the observed field-to-field scatter. As expected, the most discordant distributions come from the two smallest fields (BR1202 and VLTTC). For the purpose of the KC98 test, what is critical is the number of massive high z galaxies detected in the sample. Only 9% of the galaxies are found at $z \geq 1.6$ (8%, 7% and 12% in the NTTDF, HDF-N and HDF-S respectively), and only 5% at $z \geq 2$ (6%, 4% and 2%). A similar conclusion was reached by Saracco et al 1999.

In the lower panel, the total distribution is compared to the predictions of PLE models (as adopted from KC98) and of the CDM models described in the previous section. All the CDM models are reasonably consistent with each other, despite the wide variety of cosmological and physical parameters adopted. As expected, the Open and the Λ models predict the slower evolution. Conversely, there is a large difference between the ensemble of hierarchical models and the PLE predictions in the KC98 rendition. This fact, that was already stressed by KC98, applies not only to the SCDM used by KC98 but also to other models with different cosmologies, strengthening the validity of the KC98 test.

A main result of this paper is that *the observed cumulative distribution is in good agreement with that predicted by the hierarchical models*, strongly supporting hierarchical scenarios where massive objects are the result of merging processes in recent epochs.

To reiterate that the $K \leq 21$ threshold corresponds to a selection with respect to the mass of the galaxies we have labelled the upper x-axis of Fig.1 with the mass in stars contained in an evolved galaxy at the corresponding redshift, normalized to $K=21$. At $z \geq 1.6$, the minimum mass in stars in objects at $K \leq 21$ is $\simeq 10^{10} M_\odot$. However, a significant

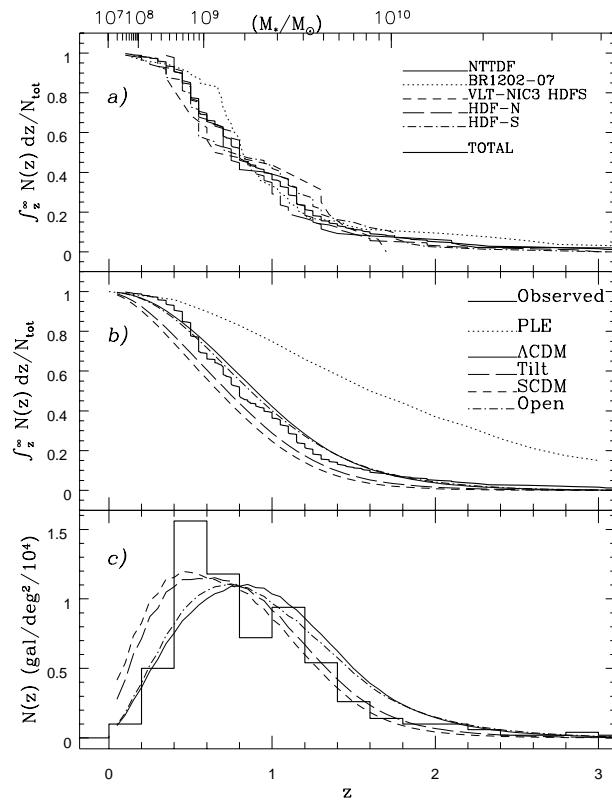


Figure 1. Redshift distribution at $K \leq 21$. *a)* Observed normalized cumulative distribution of a total of 391 galaxies in five fields. Thin lines: individual distributions (see legend for details). Thick line: total distribution. *b)* Comparison between the total cumulative distribution of the upper panel with theoretical predictions of the four CDM models described in the text and of the PLE model. *c)* Comparison between the observed differential redshift distribution and the CDM predictions. The upper axis of panel *a* shows the mass in stars contained in an evolved galaxy at the corresponding redshift, normalized to $K=21$. A Miller-Scalo IMF, age of 2Gyr, solar metallicity and star-formation timescale of 0.1 Gyr were adopted.

contribution to the K luminosity may also be due to the AGB population during a starburst phase. For comparison, the same $K=21$ luminosity may be obtained from a $z = 1.6$ galaxy of only 0.1 Gyrs of age with a constant star formation rate of $10 M_\odot/\text{yr}$ (and hence a mass of $10^9 M_\odot$). In conclusion, both massive evolved objects and/or strong starbursts may contribute to the counts at $z \geq 1.6$ and $K \leq 21$. Since both classes are relatively rare in “bottom-up” hierarchical models, the redshift distribution is a sensitive test of these models.

The agreement between the observed and predicted distribution is slightly worse at $z \leq 0.5$. The observed differential distribution (Fig.1c) has indeed a paucity of galaxies at very low redshifts with respect to the theoretical predictions, an effect that produces the steeper cumulative distribution shown in Fig.1b. This is likely to be a combination of selection effects (these small fields have been explicitly chosen to be free of bright local galaxies) and of the slope of the faint end of the luminosity functions in CDM models, that is steeper than locally observed.

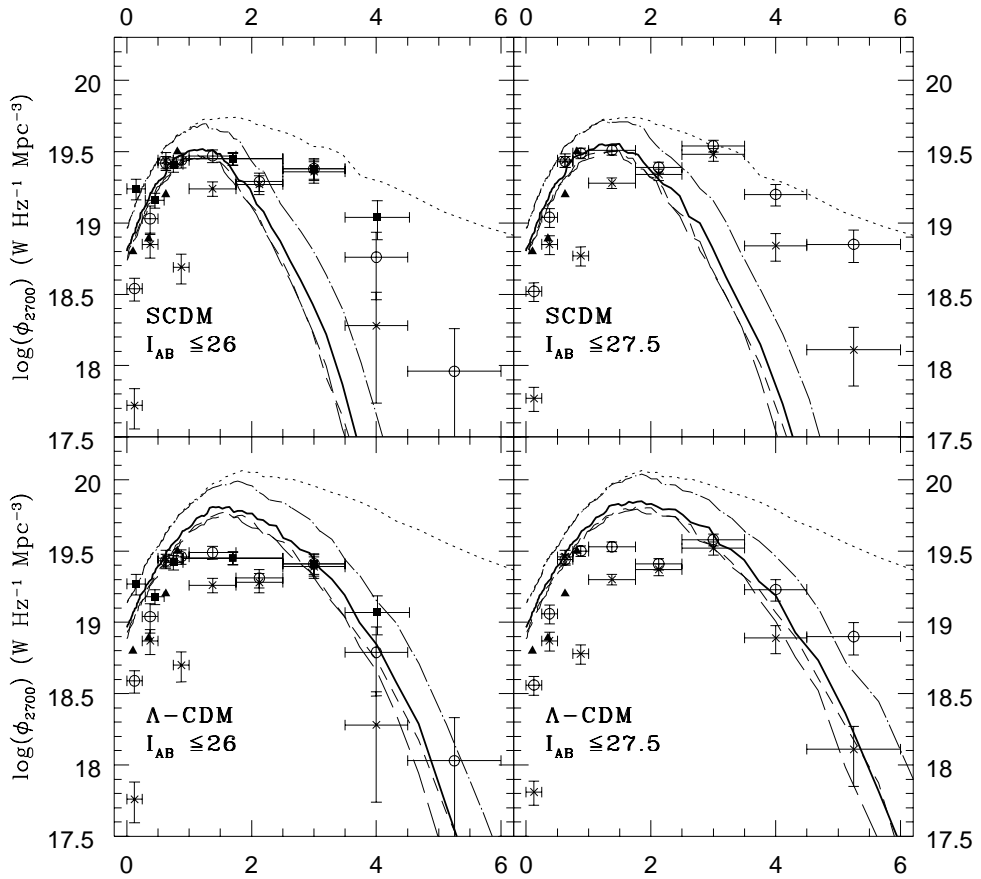


Figure 2. A comparison between the observed evolution of the luminosity density ϕ_{2700} and the predictions of hierarchical models. Empty circles are derived from the HDF-N, crosses from the HDF-S and filled squares from the NTTDF. Points are *not* corrected for incompleteness. Errorbars are computed from the number of objects in the bins, assuming simple Poisson statistics. Triangles are taken from the spectroscopic surveys of Treyer et al; 1997 (lowest bin) and Lilly 1995. From left to right two different magnitude limits have been adopted as shown in the figures. Upper panels are for standard CDM, lower panels for a Λ dominated Universe. Theoretical curves are computed with our analytical rendition of hierarchical models for the relevant cosmology. Dotted line is the total UV luminosity density computed from the models assuming no dust absorption; dashed-dot line is the same quantity when a magnitude cut corresponding to the magnitude limit in the data is applied; thick solid: magnitude cut + dust absorption (Calzetti); short dashed: magnitude cut + dust absorption (SMC) ; long dashed: magnitude cut + dust absorption (MW)

4 THE COSMOLOGICAL EVOLUTION OF THE UV LUMINOSITY DENSITY

We show in Fig.2 the cosmological evolution of the UV luminosity density ϕ_{2700} as estimated from the photometric redshifts at $I_{AB} \leq 26$ (HDF-N + HDF-S + NTTDF, left panels) and at $I_{AB} \leq 27.5$ (HDF-N + HDF-S, right panels), for two different cosmologies. The L_{2700} luminosity of each galaxy in the sample is directly obtained from the best-fitting spectrum, and falls in the range of the observed magnitudes at any redshift $z > 0.25$. At $z > 2.4$, most objects are undetected in the IR bands, and the fitting spectra are constrained by the corresponding upper limits.

The availability of these three different fields allows us

for the first time to compare the evolution of ϕ_{2700} in different fields. At $I_{AB} \leq 26$ the NTTDF is in good agreement with the HDF-N, while the HDF-S shows significant differences at $0.75 < z < 1.5$ and at $z > 3.5$, due to the variance in the total counts and in the redshift distributions. At this stage, it is not clear whether the overall discrepancy among the fields, and most notably between HDF-N and HDF-S, is due to a real cosmic variance or to some instrumental effect, and we consider it as an estimate of the global uncertainties in this analysis. At $z \leq 1.5$, the results from the NTTDF and the HDF-N are consistent with those from spectroscopic surveys (Treyer 1998, Lilly 1995) when the corrections for steep luminosity functions are adopted, as seems appropriate for fields dominated by blue star-forming galaxies. At higher z

all the fields concur to a scenario where the UV luminosity density is relatively constant from $z = 1$ to $z = 4.5$.

The overall picture emerging from Fig.2 is that the UV luminosity density does not change by more than a factor of 4 over the redshift range $0 < z < 4.5$, the only exception being the $z \simeq 4$ redshift bin in the HDF-S (but see below).

The comparison with CDM models is less straightforward here. We have overplotted in Fig.2 the prediction of two well-studied examples, the SCDM and Λ -CDM. At variance with previous works, we have not corrected the observed values for incompleteness or extinction, but rather we have explicitly shown the differential effects of the inclusion of a magnitude limit and different dust extinction curves on the theoretical expectations. The comparison shows that the ϕ_{2700} overall shape is hardly recovered by the current CDM models. In particular, the SCDM model is not able to produce the density of UV photons that is observed at $z \geq 3$, while Λ -CDM is in better agreement at $3 \leq z \leq 4.5$, but predicts a pronounced peak at $z \simeq 1.5$ and a drop by a factor of 8 from $z = 1.5$ to $z = 4$ that is not observed in the data.

A more accurate comparison at high redshift can be carried out by plotting (Fig.3) the redshift evolution of the UV luminosity density at a shorter wavelength (1400 Å), where the best-fitting spectra are tied to the observed R and I bands, and comparing it with spectroscopic surveys and CDM models. Photometric surveys are consistent with the results of spectroscopic surveys on brighter samples with the exception of the HDF-S, especially at $z \geq 3.5$. The large variance between the HDF-N and the HDF-S is due to an intrinsic lack of high redshift galaxies in the latter. In particular 4 objects are identified at $z \geq 5$ in the HDF-N, while no convincing candidate is found in the HDF-S, after removing obvious stars. It should be noted that when a standard color selection as in Madau et al. (1996) is applied, a comparable number of B-dropout galaxies can be found in the HDF-N and -S. However, these represent only a fraction of the high redshift galaxies found by the photometric redshift technique (see Pascale et al. 1998, Fontana et al. in preparation) that uses the IR bands as additional constraints. These additional high- z candidates are brighter and more numerous in the HDF-N than in the HDF-S, producing the different values shown in Fig. 3.

5 SUMMARY

We have collected and analyzed a sample of 1712 I-selected and 319 $K \leq 21$ galaxies from public deep imaging surveys, mainly the two HDFs and the NTTDF. We have derived photometric redshifts for the whole sample in an homogeneous way. The results may be summarized as follows:

- The redshift distribution of the $K \leq 21$ sample (Fig. 1) is dominated by objects at low or intermediate redshift, with a fraction of only 9% of galaxies detected at $z \geq 1.6$ and of 5% at $z \geq 2$;
- The UV luminosity density ϕ_{2700} is confined within a factor of 4 from $z = 0$ to $z = 4.5$ (Fig.2), and is relatively constant from $z = 1$ to $z = 4.5$, although significant field-to-field variations exist and dominate over statistical uncertainties;

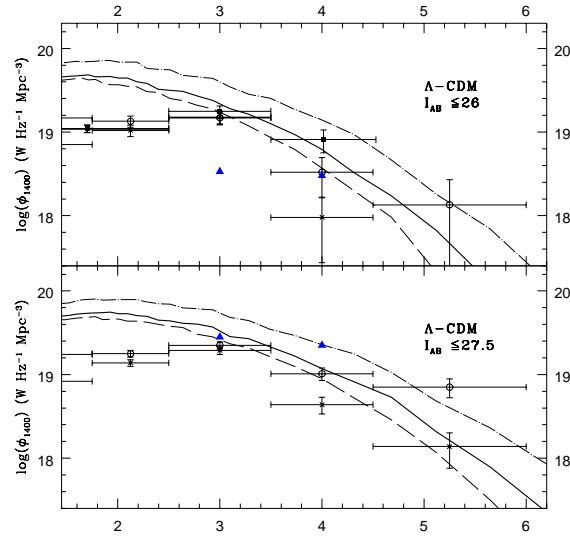


Figure 3. A comparison between the observed evolution of the luminosity density ϕ_{1400} and the prediction of hierarchical models. Triangles in the upper panel are from spectroscopic data of Steidel et al. (1999). These have been corrected for incompleteness up to $I_{AB} = 27.5$ in the lower panel. All the other symbols and lines as in Fig. 2

- A comparison between HDF-N and HDF-S shows that the UV luminosity density ϕ_{1400} at $z \geq 4.5$ is still poorly determined, probably due to the cosmic variance between these two small fields. ϕ_{1400} changes by a factor of $\simeq 6$ between the two fields at $z \geq 4.5$, since no convincing $z \geq 5$ candidate is found in the HDF-S, compared to 4 in the HDF-N (2 of which have spectroscopic confirmation).

We have compared these results with the predictions of our analytical rendition of popular CDM models. We chose not to correct the data for incompleteness or dust extinction, but rather to include both effects in the theoretical model we compare with.

The $K \leq 21$ redshift distribution at $z \geq 1$ directly reflects the number of massive galaxies already assembled at $z \geq 1$ (KC98). The agreement that we find between the observed distribution and the prediction of an ensemble of CDM models (Fig.1b) strongly supports a key feature of these theoretical scenarios, i.e. that massive objects are the result of merging processes in recent epochs.

On the other hand the overall shape of the UV luminosity density, that is tied to the physical mechanisms driving the star formation processes, is not easily reproduced by current CDM models. The comparison between the observed evolution and the prediction of two different models (SCDM and Λ -CDM) shows that the SCDM model is not able to produce the density of UV photons that is observed at $z \geq 3$. Given the $I_{AB} \leq 27.5$ limit applied to both observations and models, the discrepancy means that the current SCDM model fails to reproduce the bright tail of the luminosity function. Λ -CDM is in better agreement at $3 \leq z \leq 4.5$, but predicts a pronounced peak at $z \simeq 1.5$ and a drop by a factor of 8 from $z = 1.5$ to $z = 4$ that is not

observed in the data. Such a result holds for all the adopted extinction laws. This implies that further refinements are required in the treatment of the physical processes directly related to the SFR. For instance, adopting a weaker feedback would increase the luminosity of fainter galaxies that dominate the statistics at $z \geq 2$ yielding a less steep decline of the SFR. Another possibility is that merging activity at $z \geq 2$ is effective in enhancing the luminosity and/or the number density of faint galaxies at such z . A first attempt to include these effects has been described by Somerville, Primack and Faber 1998. These - or other - changes will require a global recalibration of the model parameters, in order to fit the increasing number of observables at low and high redshift.

Acknowledgments

We thank Alvio Renzini for stimulating discussions on this research topics, the referee, Guinevere Kauffmann, for several useful comments which improved the paper and F. Governato, S. Savaglio and V. Testa for comments on earlier versions of this work. The paper is based on observations made with: the ESO VLT Antu telescope at the Paranal Observatory, the ESO New Technology Telescope at the La Silla Observatory (some of which under the EIS programs 59.A-9005(A), 60.A-9005(A)), the NASA/ESA Hubble Space Telescope and the Kitt Peak National Observatory. The ultraviolet observations of the NTTDF were performed in SUSI-2 guaranteed time of the Observatory of Rome in the framework of the ESO-Rome Observatory agreement for this instrument.

gear, W., Oliver, S., Lawrence, A., Longair, M.m Goldsmith, P., Jenness, T. 1998, *Nature*, 394,241
 Kauffmann, G., White, S. D. M., Guiderdoni, B., 1993, *MNRAS*, 264, 201
 Kauffmann, G. and Charlot, S., 1998, *MNRAS*, 297, L23 (KC98)
 Lacey, C., Cole, S., 1993, *MNRAS* 262, 627L
 Lilly, S. J., Tresse, L., Hammer, F., Crampton, D., & Le Fèvre, O. 1995 *ApJ*, 455, 108
 Madau, P., 1995, *ApJ*, 441, 18
 Madau, P., Ferguson, H. C., L., Dickinson, M., Giavalisco, M., Steidel, C. C., Fruchter, A., 1996 *MNRAS*, 283,1388
 Madau, P., Pozzetti, L., Dickinson, M., 1998, *ApJ*, 498, 106
 Menci, N., Cavaliere, A., 1999, *MNRAS* subm.
 Pascale, S. M., Lanzetta, K. M., Fernandez-Soto, A., 1998, *ApJ* 508, L1
 Pei, Y. C. 1992, *ApJ*, 395, 130
 Poli, F., Giallongo, E., Menci, N., D'Odorico, S., Fontana, A., 1999, *ApJ* in press.
 Saracco, P., D'Odorico, S., Moorwood, A., Buzzoni, A., Cuby, J.-G., Lidman, C. 1999, *A&A*, in press
 Schade D., Lilly, S. J., Crampton, D., Ellis, R. S., Le Févre, O., Hammer, F., Brinchmann, J., Abraham, R., Colless, M., Glazebrook, K., tresse, L., Broadhurst, T., 1999 *ApJ* in press, astro-ph/9906171
 Somerville, R. S., & Primack, J. R. 1998, *MNRAS* submitted, astro-ph/9802268
 Somerville, R. S., & Primack, J. R. , Faber, S., M. 1998, *MNRAS* submitted, astro-ph/9806228
 Steidel, C. C., M., Adelberger, K. L., Giavalisco, M., Dickinson, Pettini, M., 1999, *ApJ* 519, 1
 Treier, M. AQ., Ellis, R. S., Milliard, B., Donas J., Bridges, T. J. 1998, *MNRAS*, 300, 303
 White, S., D. M., & Frenk, C. S. 1991, *ApJ*, 379, 52

REFERENCES

Arnouts, D'Odorico, S., Cristiani, S., Zaggia, S., Fontana, A., Giallongo, E., 1999a, *A&A* 341, 641
 Arnouts, S., Cristiani, S., Moscardini, L., Matarrese, S.,Lucchin, F., Fontana, A., Giallongo, E., 1999b, *MNRAS* in press, astro-ph/9902290
 Baugh, C. M., Cole, S., Frenk, C. S., Lacey, C. G., 1998, *ApJ*, 498, 504
 Bernardi, M., Renzini, A., da Costa, L. N., Wegner, G., Alonso, M. V., Pellegrini, P. S., Rite', C., Willmer, C. N. A., 1999, *ApJ*, 508, 143
 Cohen, J. G., Blandford, R., Hogg, D. W., Pahre, M. A., & Shopbell, P. L. 1999, *ApJ*, 512, 30
 Cole, S., Aragón-Salamanca, Frenk, C. S., Navarro, J. F., Zepf, S. E., 1994, *MNRAS*, 271, 781
 Connolly, A. J., Szalay, A. S., Dickinson, M., SubbaRao, M. U., & Brunner, R. J. 1997, *ApJ*, 486, L11
 Cowie, L. L., Songaila, A., Barger, A. J. 1999, *AJ* in press, astro-ph/9904345
 Cowie, L. L., Songaila, A., Hu, E. M., Cohen, J. G. 1996, *AJ*, 112, 839
 Da Costa, L. et al , 1998, *A&A* subm. astro-ph/9812105
 Fernandez-Soto, A., Lanzetta, K. M., Yahil, A, 1999, *ApJ* 513, 34
 A. Fontana A., D'Odorico S., Fosbury, R., Giallongo, E., Hook, I., Poli, F., Renzini, A., Viezzer R., , 1999, *A&A* 343, L19
 Giallongo, E., D'Odorico, S., Fontana, A., Cristiani, S., Egami, E., Hu, E., McMahon, R. G., 1998, *AJ* 115, 2169 (G98)
 Guiderdoni, B., & Rocca-Volmerange, B. 1987, *A&A*, 186, 1
 Heyl, J. S., Cole, S., Frenk, C. S., Navarro, J. F., 1995, *MNRAS*, 264, 755
 Hughes, D.H., Serejeant, S., Dunlop, J., Rowan-Robinson, M., Blain, A., Mann, R. G., Ivison, R., Peacock, J., Efstatithou, A.,